Implantation and erosion of nitrogen in tungsten

2014 New J. Phys. 16 093018

(http://iopscience.iop.org/1367-2630/16/9/093018)

New Journal of Physics
The open access journal at the forefront of physics
Deutsche Physikalische Gesellschaft DPG | IOP Institute of Physics

Implantation and erosion of nitrogen in tungsten

G Meisl[1], K Schmid[1], O Encke[1], T Höschen[1], L Gao[1] and Ch Linsmeier[2]
[1] Max-Planck-Institut für Plasmaphysik, Boltzmannstraße 2, D-85748 Garching, Germany
[2] Forschungszentrum Jülich GmbH, Institut für Energie- und Klimarforschung-Plasmaphysik, D-52425 Jülich, Germany
E-mail: gmeisl@ipp.mpg.de

Received 2 May 2014, revised 24 June 2014
Accepted for publication 21 July 2014
Published 15 September 2014
New Journal of Physics **16** (2014) 093018
doi:10.1088/1367-2630/16/9/093018

Abstract
Nitrogen puffing is routinely applied in nuclear fusion plasma experiments with tungsten walls to control the amount of power emitted from the plasma by radiation. However, as nitrogen is retained in significant amounts in tungsten it adds some complexity to the plasma-wall interaction. Basic questions concerning the interaction of nitrogen with tungsten, namely the energy and temperature dependent retention of nitrogen implanted into tungsten and the erosion of the formed tungsten nitride by deuterium, are still open. To address these questions, laboratory experiments with a mass-filtered ion source and sample analysis with *in situ* x-ray photoelectron spectroscopy (XPS) and nuclear reaction analysis were performed. The results of the implantation and erosion measurements were interpreted by means of simulations with a Monte-Carlo code describing the interaction of energetic particles with matter in the binary collision approximation. This required the development of a forward calculation, converting the simulated depth profiles into XPS intensity ratios. With appropriate settings, the experimental implantation and erosion results at ambient temperature are well described by the simulations. However, for increased temperatures it has been observed that there is an unexpected difference between implanting nitrogen into tungsten before heating the sample and implantation into a heated sample. The application of the developed forward calculation is not

limited to the problems presented in this work but can be applied especially to all kind of XPS sputter-depth profiling measurements. Finally, simulations with the previously validated Monte-Carlo code are used to extrapolate the presented results on nitrogen retention to energies and particle compositions relevant for fusion experiments. These simulations make quantitative predictions on nitrogen retention in tungsten and on relevant time scales. The simulations also show that recoil implantation of nitrogen by deuterium significantly increases the effective implantation depth of nitrogen.

Keywords: plasma-wall interaction, tungsten nitride, XPS quantification, sputter-depth profiling, SDTRIMSP

1. Introduction

In magnetic fusion experiments a hydrogen plasma is confined by magnetic fields and heated to very high temperatures to initiate nuclear fusion reactions. The part of the heating power transported to the wall along the magnetic field lines hits a very narrow region, the divertor target plates. The resulting power flux densities can even exceed the power handling capabilities of tungsten (about 5 MW/m^2), which is currently the favored material for divertor target plates. The power flux can be distributed more evenly on the walls by radiation emitted from the edge plasma. In fusion experiments like ASDEX Upgrade and JET, puffing of nitrogen or noble gases is mandatory at high heating powers to avoid excess power fluxes to the divertor targets [1].

Nitrogen has favorable radiation properties, which keep the radiation low in the hot, central plasma, but reduce the power flux to the divertor targets [2]. Conveniently, nitrogen also enhances plasma performance [2]. However, nitrogen is special in its interaction with the walls. Different from hydrogen or noble gases, it can be retained in a notable amount by forming compounds like tungsten nitrides, W_xN, in the implantation zone. On the other side, as nitrogen is a gas, no layers of pure nitrogen can be deposited on top of the original wall material. This means that initially the walls act as a pump for nitrogen. When the walls are saturated with nitrogen all incident nitrogen is reemitted in the recycling flux.

The physical sputtering process of tungsten by nitrogen seems to be understood [3, 4]. Also the deposition of tungsten nitride films for industrial applications, like microelectronics, has been studied in some detail [5, 6]. In contrast, results on the temperature dependence of formation and stability of tungsten nitride layers created by nitrogen implantation are contradictory [3, 7]. The temperature stability of tungsten nitride is an important aspect for the application of nitrogen in fusion experiments, as a sudden release of large amounts of nitrogen from the walls could terminate the plasma operation. The erosion of tungsten nitride layers by deuterium, the most abundant species in fusion plasmas, has not been measured yet. An improved understanding of these processes is desirable to deduce the nitrogen fluxes in the plasma, to predict the erosion of the walls and the hydrogen retention [8, 9], and to improve the feedback control for radiative cooling.

Therefore comprehensive studies have been carried out, combining laboratory experiments and fusion experiments, as well as computer simulations. The present contribution summarizes

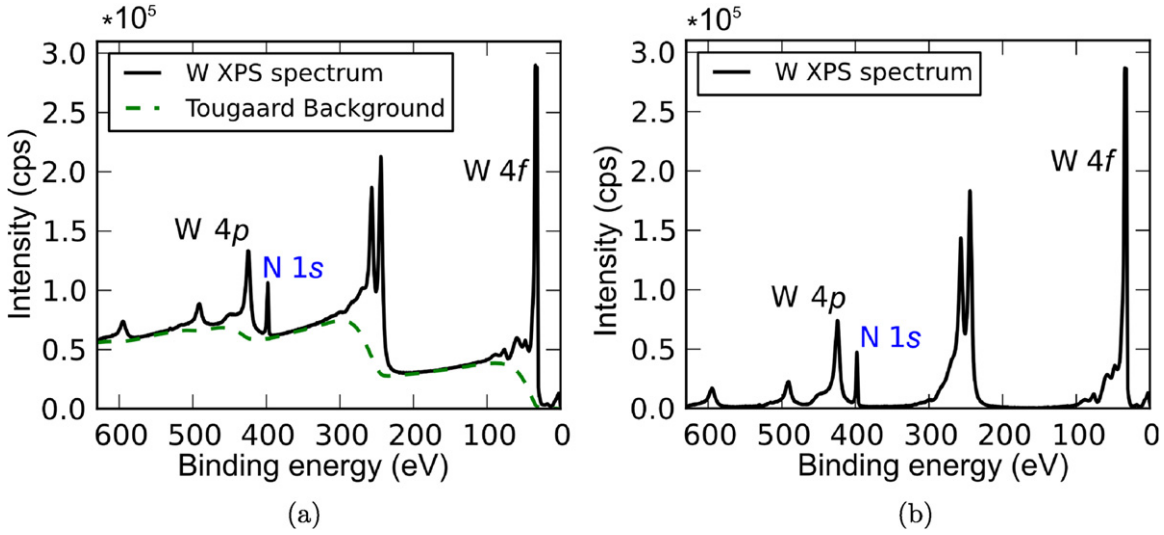

Figure 1. XPS spectrum of N-ion implanted W. (a) Original spectrum with the important peaks labeled. (b) Spectrum after background subtraction.

results from laboratory experiments. In these experiments, methods from surface analysis were used to gain further insights into nitrogen (N) accumulation and stability in tungsten and the erosion of W_xN under deuterium bombardment. The experiments were performed in a UHV system equipped with x-ray photoelectron spectroscopy (XPS), which allows following the surface composition evolution *in situ* during heating ramps or ion bombardment. In order to check the agreement between experimental measurements and dynamic Monte-Carlo simulations with the SDTRIM.SP code (see section 2.3), a detailed model was developed to calculate XPS intensities from SDTRIM.SP depth profiles.

2. Methods

2.1. Experimental setup

For the experiments we employed hot rolled tungsten (W) samples with a purity of 99.97 wt.% produced by PLANSEE[3], polished to a mirror-like surface finish and annealed in vacuum at 1200 K for 2 h.

The experiments were performed in a commercial XPS device, PHI ESCA 5600 with OmniFocus III lens. The base pressure was in the 10^{-8} Pa range. All measurements except for one were done using monochromated Al Kα radiation and an angle of 90° between the incoming monochromatic X-ray radiation and the hemispherical electron energy analyzer. For the measurement shown in figure 12 a non-monochromatic Mg Kα source was used with an angle between X-ray source and detector of 54.7°. The pass energy was 93.9 eV for all presented measurements.

The XPS device is equipped with sample heating and two SPECS IQE 12/38 ion sources for *in situ* ion implantation. One of the ion sources is equipped with a Wien filter and was used

[3] This is the same material from the same manufacturing batch as already employed for the work described in [8] and as material WP in [7].

for implantation with 5 kV acceleration voltage. As the beam consisted of N_2^+, the resulting energy per atom was 2.5 keV. Due to technical problems implantation at 500 eV per atom was performed with the unfiltered ion source. Analysis of the mass-filtered beam showed that already the unfiltered beam consists of at least 99% N_2^+, little N^+, and traces of impurities like argon or hydrogen. The deuterium (D) bombardment was performed with D_2^+ from the mass-filtered ion source at an energy of 2.5 keV per deuterium atom. The angles of the mass-filtered and unfiltered ion sources to the sample surface normal are 45° and 40°, respectively.

The N ion fluence on the samples was deduced from measurements of the sample current during the implantation. The sample current was measured with a bias of 50 V to suppress secondary electrons. This voltage was sufficient to give a good agreement with measurements of the ion fluence by a Faraday cup. The mass-filtered ion beam had a Gaussian profile with a full-width-at-half-maximum of about 0.5 mm. The ion source without mass filter had a larger beam, with a full-width-at-half-maximum of about 1.5 mm. For the N implantation both beams were scanned over an area of 6 mm by 6 mm to ensure a homogeneous implantation. The XPS analysis area is circular with a diameter of 0.8 mm. The area used for the fluence calculation was $6.5 \times 6.5\,\mathrm{mm}^2$. To reach the fluences for the D erosion measurements within reasonable time, the bombarded area was reduced to $9\,\mathrm{mm}^2$. With this smaller area the fluence is not entirely homogeneous over the bombarded area. Therefore the D fluence was deduced from current measurements with a Faraday cup. However, a lateral scan by XPS subsequent to the D bombardment confirmed that the erosion was homogeneous within the XPS analysis area.

To determine the integral amount of N after implantation, nuclear reaction analysis (NRA) was performed on selected samples. The protons emerging from the nuclear reaction $^{14}\mathrm{N}\left(^4\mathrm{He},^1\mathrm{H}\right)^{17}\mathrm{O}$ with a ^{4}He energy of 4.80 MeV were counted in a detector with a solid angle of 29.95 msr at a scattering angle of 135°. A cross section has been determined for this setup by measurements of a CN_x layer, with an N areal density known from Rutherford backscattering (RBS) measurements [10]. According to this cross section a count rate of $1\frac{^1\mathrm{H}}{\mu C}$ for 4.80 MeV $^4\mathrm{He}^{1+}$ corresponds to an areal density of $1.6 \times 10^{15}\frac{^{14}\mathrm{N}}{\mathrm{cm}^2}$.

2.2. Evaluation of XPS measurements

For a quantitative analysis of XPS measurements, the relative peak intensities (i.e. peak areas) must be determined. This task consists of two main steps: first, the background caused by inelastically scattered electrons must be removed. Second, the remaining signal must be attributed to the different peaks. Both steps require some care. An XPS spectrum from an N-implanted W sample is shown in figure 1(a). The analysis in the present work focuses on the N 1*s* peak at 398 eV and the most intense tungsten peak, W 4*f* around 33 eV. A sketch of all the steps taken in the evaluation of the measured intensities is given in the appendix in figure 16. Also the method used to separate the N 1*s* from the W 4*p* peak can be found in appendix A.

Background subtraction Two widely used types of backgrounds for XPS spectra of metals are the Shirley background [11] and the Tougaard background [12]. The Shirley background can be applied even when only the peak areas have been measured. Mainly because start and end points of the background calculation are chosen individually for each peak, the derived intensities may be flawed. The Tougaard background is based on a physical model which improves the accuracy in comparison to the Shirley background [13]. However, it is only applicable to spectra which cover a wide energy range.

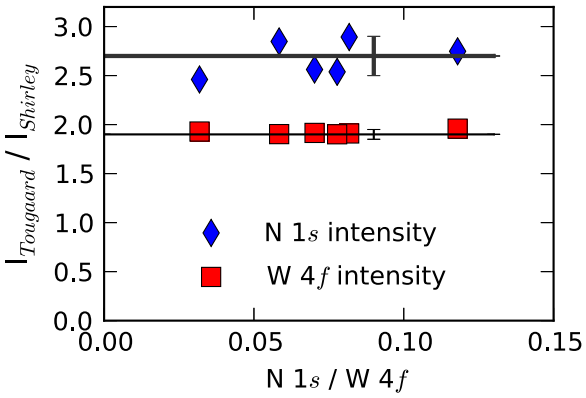

Figure 2. The intensities from Shirley and Tougaard background subtraction have a constant ratio of 1.9 for W 4*f* and 2.7 for N 1*s*.

As can be seen in figure 1(a) the inelastic background could be well fitted with a Tougaard background with the standard parameters $B = 2866$ and $C = 1643$ [14]. The intensity of the W 4*f* peak was determined by integrating the background subtracted spectrum from 21.5 to 130 eV[4].

Calibration factor for Shirley background To reduce the effort required for further measurements[5], another step was taken: for the set of spectra for which the N 1*s* intensity was determined according to appendix A, the N 1*s* and W 4*f* peak intensities were additionally determined by subtracting a Shirley background. The ratios of the intensities determined from the procedure using Tougaard backgrounds to the ones determined with a Shirley background are shown in figure 2. Using these ratios as calibration factors, it is finally possible to determine intensity ratios with the Shirley background, where the dependence on user chosen parameters has been eliminated and the contributions to the N 1*s* peak located in the region of the W 4*p* peak are included. Exploiting the advantage of the Shirley background, that the measurement of small energy intervals is sufficient, allowed us to reach good counting statistics in a short time. The derived calibration factors change the intensity ratio N 1*s* /W 4*f* by the factor 2.7/1.9 = 1.4. That means a direct use of the intensities based on a Shirley background subtraction underestimates the intensity ratio by 40%.

2.3. Forward simulation of XPS intensity ratios from SDTRIM.SP depth profiles

SDTRIM.SP The transport of energetic particles in matter can be described in the binary collision approximation (BCA) in combination with electronic stopping [15]. In the energy range below 50 eV additional processes, like attractive interaction between particles or simultaneous interaction of more than two particles, can become important. Codes like SDTRIM.SP [16, 17] based on the binary collision approximation are well tested and routinely applied. SDTRIM.SP simulates the transport of energetic particles in amorphous solids with a Monte Carlo approach. The quality of SDTRIM.SP results depends on input parameters and the

[4] This range also includes the small W 5*s* and W 5*p* peaks. Consequently these peaks are included in the forward calculation with a contribution of about 10% to the intensity.

[5] The measurement of a large energy interval required for the application of the Tougaard background increases the required integration time with detrimental effects on the cleanliness of the surface and number of available measurements.

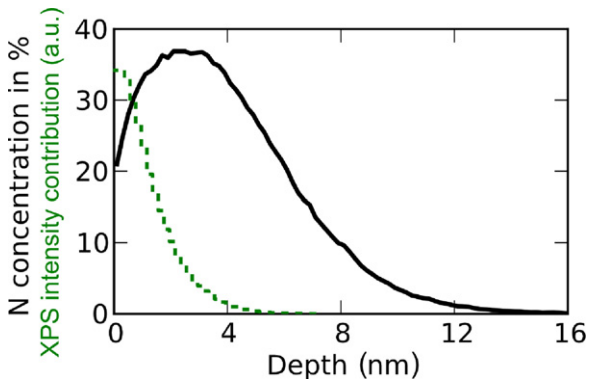

Figure 3. Calculated N depth profile for 2.5 keV N implantation; the dashed line represents the contributions from different depths to the measured XPS intensity, i.e. the contributions to the sum in equation 3.

kinetic energy which should be above 50 eV. Since diffusion and chemical effects become more important with increasing temperature, the best agreement of SDTRIM.SP with experimental results can be expected for low temperatures. A depth profile calculated by SDTRIM.SP for the implantation of N into W is shown in figure 3. The calculation was done with an energy of 2.5 keV at 45° and a surface binding energy for N which varied with the surface composition from 4.4 eV (pure W) to 3.5 eV (with N).

For the erosion of nitrogen from a surface by ion bombardment, physical sputtering described by SDTRIM.SP defines the minimum erosion yield. Chemical interactions can present additional loss channels and could increase the loss of N. Indications for the chemical erosion of N in Be by D have been found at PISCES-B [18].

Interpretation of XPS measurements XPS measurements are weighted averages over a depth of roughly three electron inelastic mean free paths (IMFP). The weight function is an exponential, strongly emphasizing the contribution from the surface. Quantification of XPS results based on the simple application of relative sensitivity factors is naturally not possible for inhomogeneous materials. Inversion of the exponentially weighted average for depth resolved XPS measurements is difficult [19]. Also the measurement of the N depth profile by RBS, as performed for N implanted into Be [20], is not possible in a W matrix. In contrast, the conversion of a given depth profile (assuming lateral homogeneity) to XPS intensity ratios is possible by applying the formula

$$I_A = \sigma_A \cdot L_A \cdot \Gamma_{\mathrm{Phot}} \int_0^\infty \rho_A(z) \exp\left(- \int_0^z \frac{1}{\lambda(z') \cdot \cos\alpha} \mathrm{d}z' \right) \mathrm{d}z, \qquad (1)$$

where I_A denotes the intensity of peak A per time unit, σ_A the energy dependent total cross section, L_A the angular dependence including elastic collisions calculated with the formulas in [21], $\rho_A(z)$ the depth dependent number density of the element that generates peak A, $\lambda(\rho)$ the electron IMFP (which depends on the local composition of the sample and the energy of the electrons), α the angle between detector and sample normal and Γ_{Phot} is the incident photon flux which cancels in the observation of intensity ratios. The cross sections are taken from Scofield [22], the asymmetry parameters from Yeh [23] and the electron IMFP from the G1 equation for inorganic compounds [24].

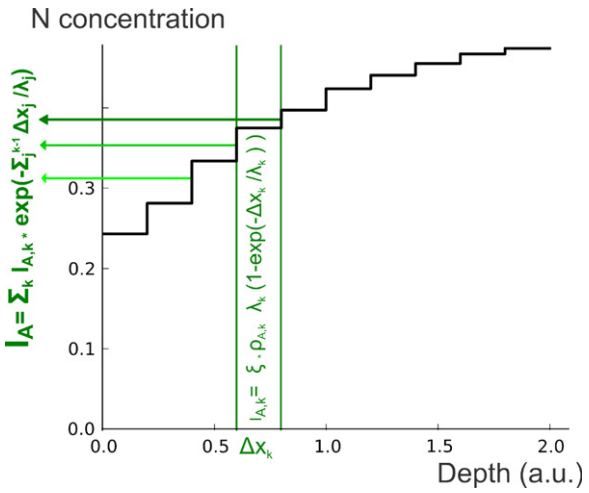

Figure 4. Illustration of XPS forward calculation.

The result of adopting equation 1 to the discrete output given by SDTRIM.SP is illustrated in figure 4. In a first step the intensity emitted from every SDTRIM.SP depth layer is calculated. Since within one SDTRIM.SP layer the composition is homogeneous, the outgoing intensity in peak A can be calculated for one single layer k analytically:

$$I_{A,k} = \xi_A \rho_{A,k} \lambda_k \left(1 - \exp\left(\frac{-\Delta x_k}{\lambda_k}\right)\right). \tag{2}$$

In this expression ξ_A contains all the prefactors, k denotes the layer, $\rho_{A,k}$ is the number density in layer k, λ_k the IMFP in layer k and Δx_k the thickness of layer k. The fraction of the intensity from layer k reaching the surface after passing through the layers 0 to $k-1$ is $\prod_{j=0}^{k-1} \exp\left(-\frac{\Delta x_j}{\lambda_j}\right)$. The contribution to the measured N 1*s* intensity from different layers, $I_{A,k} \cdot \exp\left(-\sum_{j=0}^{k-1} \frac{\Delta x_j}{\lambda_j}\right)$, is shown in figure 3 for the XPS parameters described in section 2.2. The total intensity is obtained by adding up the intensities from all layers:

$$I_A = \sum_k I_{A,k} \cdot \exp\left(-\sum_{j=0}^{k-1} \Delta x_j \Big/ \lambda_j\right). \tag{3}$$

As it is not possible to infer actual physical quantities, like the areal density, from the XPS measurements, only the actual intensity ratios are given later. To support the later results, figure 5 shows the relation between the N 1*s* /W 4*f* intensity ratio and the N areal density from the simulation of 2.5 keV N implantation (shown later in figure 7). The solid line only includes the N areal density within the uppermost 4 nm, corresponding roughly to the depth probed by XPS according to figure 3. There is a rather linear relation between this fraction of the N content and N 1*s*/ W 4*f*.[6] The relation already becomes quite nonlinear when the total N areal density is considered.

[6] This statement is not valid in general. For this example the shape of the depth profile only changes slightly with the fluence. The relation could be very different when considering arbitrary depth profiles.

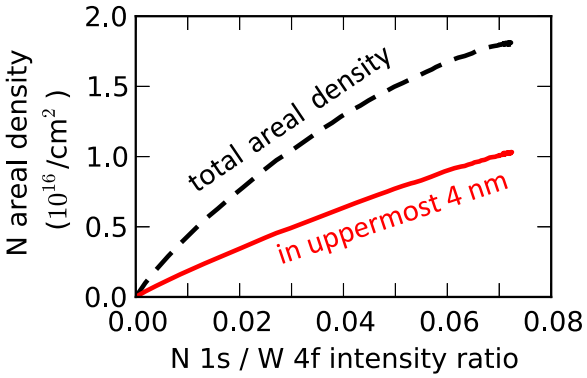

Figure 5. Relation between N 1*s* /W 4*f* intensity ratio and N areal density in all depths or within uppermost 4 nm.

The forward calculation offers the possibility to interpret XPS measurements of ion implantation by a comparison to SDTRIM.SP simulations. Deviations between measurement and simulation in the initial phase of the implantation would indicate that the reflection process is not correctly described by the binary collision approximation. For large implantation fluences the steady state is set either by the re-erosion of the implanted species or by the chemical processes limiting the maximum concentration of the implanted species (see section 3.1). If SDTRIM.SP simulations agree with the experiment at all energies and fluences, it can be assumed that SDTRIM.SP describes the implantation and erosion processes correctly.

It is often convenient to parameterize the interaction of energetic particles with matter in terms of quantities like sputter yield, reflection yield or implantation depth. After a successful benchmark it is justified to take such quantities, which are not directly accessible from our measurements, directly from SDTRIM.SP.

2.4. Uncertainties in measurements and simulations

In the comparison of experimental measurements and SDTRIM.SP simulations several sources of uncertainties exist. For experiment and simulation the integration times and number of particles, respectively, have been chosen large enough to make the statistical counting error negligible. This is reflected in the small scatter of the measurements and is demonstrated in detail for one XPS measurement.

The cross section for photo electrons for the N 1*s* peak is about a factor of 5 smaller than for the W 4*f* peak. As a worst case we consider the N 1*s* peak shown in figure 6, namely the first measurement of the 2.5 keV N implantation with a fluence of 7.8×10^{15} N cm^{-2} resulting in a N 1*s* W^{-1} 4*f* intensity ratio of 0.014, figure 7. The measurement is based on a survey spectrum where the energy range from 0 to 630 eV binding energy was measured for 190 seconds. The resulting peak consists of about 2000 counts. The peak-to-peak signal-to-noise ratio is about 4[7]. The intensity variation caused by varying the start and end points of the Shirley background is about 25%. In most of the measurements, both the integration time and N content were larger, further reducing the random error.

[7] The signal is calculated as the difference between the highest intensity of the peak to the background intensity at about 380 eV, the noise as the difference between the highest intensity to the lowest intensity in a pure noise interval around 380 eV binding energy.

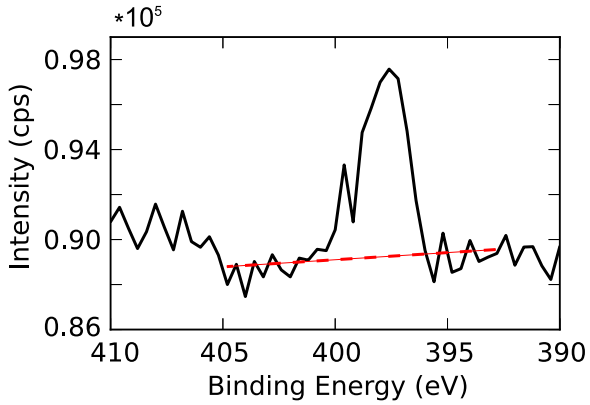

Figure 6. N 1*s* peak after a N fluence of 7.8×10^{15} N cm^{-2}. The Shirley background is a straight line because the background decreases towards higher binding energies.

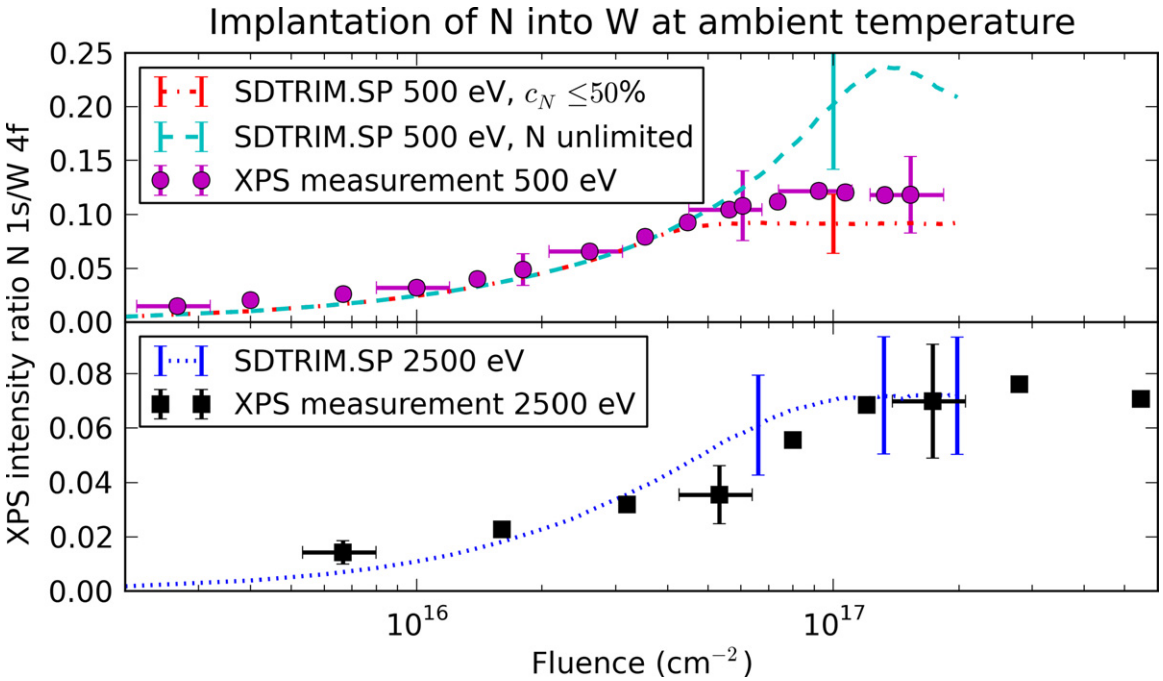

Figure 7. Implantation of N in W with 2.5 keV and 500 eV: comparison of experiment and calculated intensities according to SDTRIM.SP implantation profiles. For the simulation shown as dash-dotted curve for 500 eV N implantation the maximum N concentration was limited to 50%.

There are different sources for systematic errors in the experimental determination of intensity ratios. The uncertainty introduced by sources like sample roughness, a dependence of the transmission function on the sample position, an uncertainty in the angle between X-ray source and electron detector of $\pm 1°$, the presence of small amounts of oxygen[8] even for ultra-

[8] Small amounts of oxygen, corresponding to $\leqslant 1\%$ when evaluated via relative sensitivity factors, could be detected during and after long XPS phases like complete surveys. The oxygen was quickly removed when the samples were bombarded with N.

high vacuum conditions and stability of the device can be estimated from comparing different measurements with the same parameters on nominally identical samples: the variations observed in the W 4*s* /W 4*f* ratios for 4 clean W samples and in the N 1*s*/W 4*f* ratios after the 2.5 keV N implantations to steady state reported in this work, were about 15%.

The surface structural state was checked by scanning electron microscopy for one sample after polishing and after 2.5 keV N implantation. The bombardment by N induces a roughening on the originally smooth surfaces. For large fluences this roughening is visible by eye. The scanning electron microscopy images show generation of structures with a lateral scale of the order of 10 nm. The amplitude of the structures could not be determined from these measurements.

The overlap of the N 1*s* peak with the W 4*p* peak presents another possible source of error for the intensity determination. The evaluation described in section 2.2 reduces this uncertainty to comparably low values. From the scatter visible in figure 2 we estimate the remaining uncertainty to 15%. Considering uncertainties in the energy dependence of the detector transmission function and the observed variation in the W 4*s* /W 4*f* intensity ratio we suggest a total uncertainty of ±30% for the experimental intensity ratios.

For the experimental measurements, the uncertainty in the fluence measurement must also be considered. For the N implantations the fluence was determined by dividing the total current onto the sample by the beam spot size, as measured with the Faraday cup. From the uncertainty in the area determination we estimate the uncertainty in the fluence to ±20%. For the D implantation the slight inhomogeneities within the smaller beam spot made it necessary to measure the fluence by scanning the beam with a Faraday cup. Within the beam spot the fluence was locally up to 20% lower than in the center. A comparison of the integral of the Faraday cup measurements over the beam spot with the measured total current onto the sample suggested that the fluence measured with the Faraday cup may be up to 30% too low. Thus, the fluence uncertainty is −20% to +30%.

Systematic errors also appear in the simulation results. Especially some of the input parameters for the XPS intensity forward calculation like electron IMFP [24] and photoelectron cross section may be inaccurate. Unfortunately, the uncertainties in these input parameters are not quantified. For this reason a calculation of the error via error propagation, which is in principle possible with the forward calculation, was not performed. From published comparisons of theoretical calculations with measurements [25] and a comparison of our own calculations with peak ratios of a pure W sample the error is estimated to 30%.

For the NRA measurements, all results are based on above 100 counts, corresponding to a statistical error of $\leqslant$10%. Our cross section, based on a comparison to an RBS measurement, for the reaction $^{14}\mathrm{N}\left(^{4}\mathrm{He},^{1}\mathrm{H}\right)^{17}\mathrm{O}$ at 4.80 MeV, is 25% lower than the one published in [26].

As just discussed, most of the uncertainty is caused by systematic effects. This implies that the error is the same at least for subsequent measurements. Even though absolute values may not be that precise, the scatter within a measurement series is small and the relative behavior can be compared with significantly better accuracy.

3. Results

3.1. N implantation at ambient temperature

N ions with 2.5 keV and 500 eV per atom were implanted into W which was previously cleaned by Ar sputtering. The N content was monitored by measuring the XPS peak intensity ratio N 1*s*/ W 4*f*. The results are presented in figure 7 together with results from SDTRIM.SP simulations. For implantation at 500 eV, two SDTRIM.SP simulations are shown. They differ in the maximum allowed concentration of N, where excess N is removed from the simulation. The maximum is set to 100% (unlimited N content) for the dashed curve and 50% for the dash-dotted curve.

For the implantation at 500 eV, the simulation with a limit for the N concentration of 50% gives a good match to the measurement, while the unlimited simulation is far off. One could improve the fit by further adjusting the maximum concentration of N. However, due to the rather large uncertainty in the data such a further refinement is not justified. Nevertheless, a comparison to the simulation without limit on the N concentration shows a discrepancy which is significantly larger than the uncertainty. Based on our results (good agreement for a maximum concentration of 50%) and known phases of tungsten nitrides [5] the maximum concentration of N in W at room temperature should be between 33% and 66%.

Also for implantation at 2.5 keV, measurement and simulation agree within the uncertainty. A concentration limit would not change the result as the maximum concentration remains below 50% due to N self sputtering. The depth profile for 2.5 keV implantation calculated by SDTRIM.SP is shown in figure 3.

The previous results are also confirmed by NRA measurements after implantation. At 2.5 keV the measurement yields a nitrogen areal density of 2.3×10^{16} N cm^{-2}, which is somewhat above the areal density of 1.8×10^{16} N cm^{-2} predicted by SDTRIM.SP. At 500 eV the measurement yields an areal density of 1.1×10^{16} N cm^{-2} which is in agreement with the N areal density from the SDTRIM.SP simulation of 1.15×10^{16} N cm^{-2}.

3.2. Erosion of tungsten nitride layers with argon and deuterium

In order to study the depth distribution and erosion of nitrogen implanted into tungsten, such layers have been bombarded with argon and deuterium.

The measurement of the erosion with argon, often denoted as sputter-depth profiling, is presented in figure 8. The sample was prepared by implantation of 2.5 keV N in W at ambient temperature and then eroded by Ar bombardment at 300 and 500 K. Apart from a small difference in the initial values (see section 2.4) there is no significant difference between the measurements. In comparison to the simulation, the measured N 1*s* signal drops faster. This could indicate a shorter penetration depth of nitrogen. However, within the uncertainty, the measurements still agree with the SDTRIM.SP simulations.

In a fusion device, the species with the largest fluence impinging at plasma-facing materials are hydrogen isotopes. In our study, a W_xN layer created by 2.5 keV N implantation was eroded by 2.5 keV deuterium. Because the mass-filtered ion source was used for D, the unfiltered source was used for the N implantation. Due to the steeper implantation angle, and in agreement with SDTRIM.SP, the N 1*s*/ W 4*f* ratio after this implantation is somewhat higher than the corresponding result in figure 7. Measurement and SDTRIM.SP simulation of the D erosion experiment are shown in figure 9.

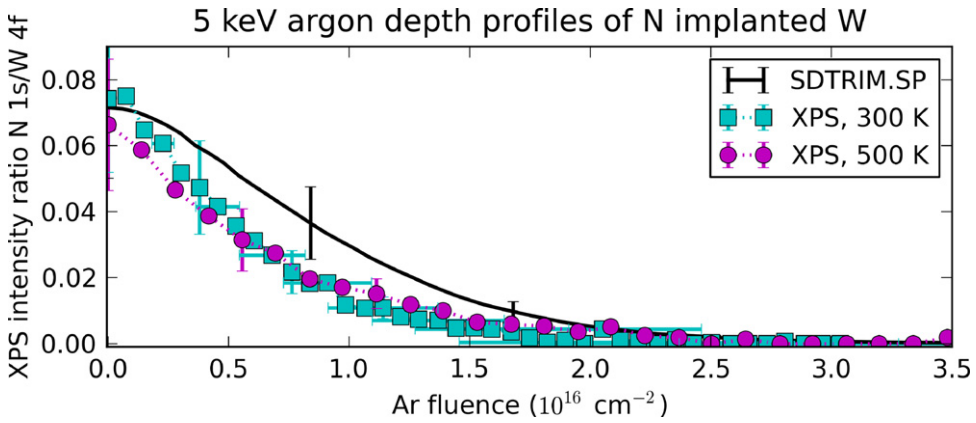

Figure 8. Erosion of W_xN layer created by 2.5 keV N implantation by argon at 300 and 500 K.

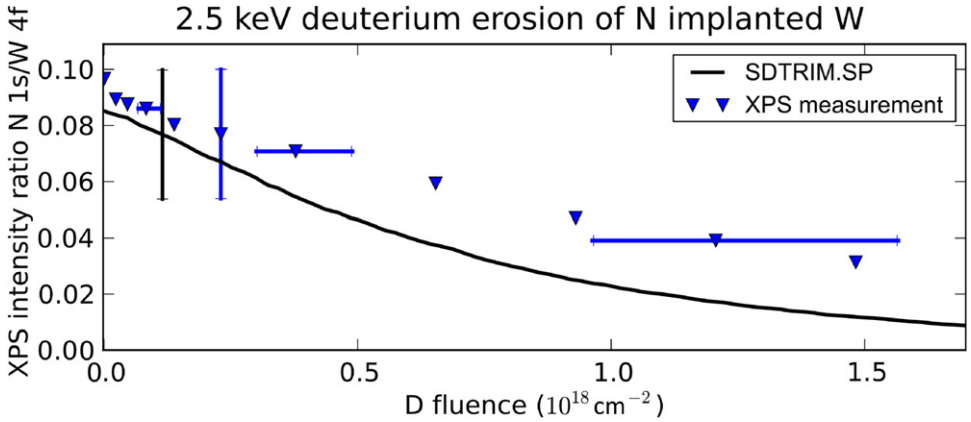

Figure 9. 2.5 keV deuterium erosion of a W_xN layer created by 2.5 keV N implantation.

Figure 9 shows a slower decay of the nitrogen content than predicted by SDTRIM.SP. The fluence required to reach a given intensity ratio in the simulation is about a factor of 2 smaller than in the measurement. In the SDTRIM.SP simulation a thickness of about 6 nm (the nitride layer is about 10 nm thick, see figure 3), has been eroded at the final fluence of 1.5×10^{18} D cm^{-2} (with a total sputter yield that drops from 0.044 to 0.022). According to SDTRIM.SP, the N erosion is limited by the fluence needed to dig through the W substrate. Therefore, a possible explanation for the discrepancy between simulation and experiment is an overestimation of W sputtering by D in SDTRIM.SP. This explanation is supported by a comparison of sputter yields from experimental measurements and simulations given in [27, p 116]. It shows that the simulated sputter yield for normal incidence of D on W around 2 keV is about a factor of two too large. As the N erosion is smaller than predicted by SDTRIM.SP, a significant chemical erosion of N by the formation of volatile molecules with D at ambient temperature can be excluded.

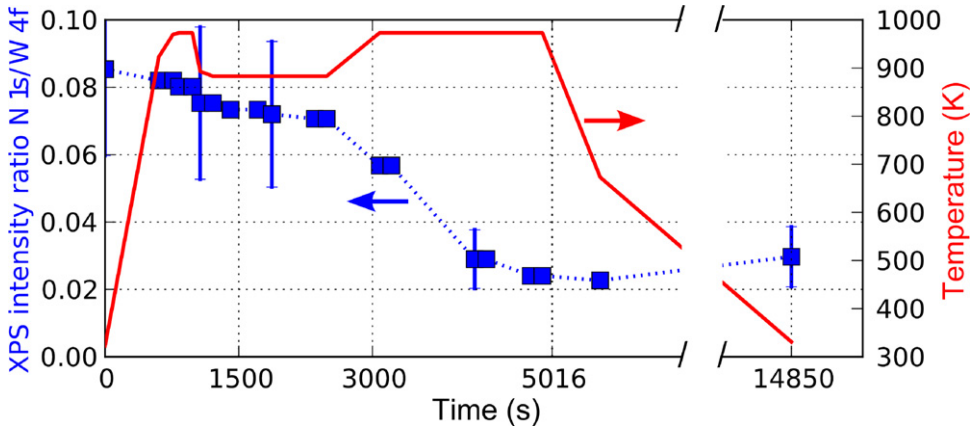

Figure 10. N 1*s*/ W 4*f* intensity ratio and sample temperature versus time.

3.3. Temperature dependence

To study the temperature dependence of N accumulation and erosion dedicated high temperature experiments were performed. In the first experiment a W_xN layer was created by implantation of 2.5 keV N at ambient temperature. Then the sample was heated and the N content in the surface of the sample was monitored with XPS. Figure 10 shows that above 900 K the N 1*s* intensity is decreasing. This decline is notably faster at 970 K. That there is no loss of nitrogen at 800 K will be discussed in figure 12.

The loss of N from the surface region accessible to XPS means that N atoms must diffuse from this region, either to the surface to recombine or further into the sample. Diffusion coefficients, based on ion implantation and subsequent heating of the sample, for N in W have been published in [28] and [29]. However, tungsten nitride is actually a reaction-diffusion system, and the tungsten nitride probably has to decompose before N atoms can start to diffuse. According to thermodynamic calculations presented in [3], WN should decompose at 600 K. This, however, has not yet been confirmed by experiments.

To check whether the result shown in figure 10 is in agreement with published diffusion coefficients of N in W, the time scale is estimated on which the diffusion changes the N content in the surface region accessible to XPS. Typically this time scale is estimated by $\tau \approx \frac{(\Delta x)^2}{D}$ with the diffusion coefficient D and the length scale Δx. This estimate is only applicable under the assumption that the complete N content can contribute to the diffusion. In contrast to that the approach described in [30] and used in [28] to derive the diffusion coefficient assumes that only solute N contributes to the diffusion. According to appendix B, a modified expression can be used to estimate the time scale:

$$\tau \approx \left(\frac{c_N}{C_0}\right)^2 \frac{\Delta x^2}{D}. \tag{4}$$

In this expression c_N is the total N concentration and C_0 the solute N concentration.

With the diffusion coefficient

$$D = 4.3(\pm 8.3) \cdot 10^{-4} \cdot \exp\left(-\frac{2.32(\pm 0.16)\text{eV}}{k_B\,T}\right)\left(\frac{\text{m}^2}{\text{s}}\right)$$

given in [28], and assuming that a layer of 10^{-8} m needs to be depleted at a temperature of 970 K by diffusion, one obtains with the common expression for the diffusion time scale: $\tau \approx \frac{(\Delta x)^2}{D} \approx \frac{\left(10^{-8}\right)^2}{5\cdot 10^{-16}}$ s ≈ 0.2 s. The solubility of N in W at 970 K given in [28] is 2.5% and the actual concentration, according to figure 3, about a factor of 15 higher. The time scale according to equation (4) is therefore 45 s. Within the error bars given for the diffusion coefficient, the time scale goes up by almost two orders of magnitude to about 2000 s (including the solubility correction) for $D = 1 \times 10^{-4} \cdot \exp\left(-\frac{2.5\text{ eV}}{k_B T}\right)\frac{\text{m}^2}{\text{s}}$. This is comparable to the observed timescale of about 1000 s.

Another value for the diffusion coefficient of N in W was published in [29]. This study is based on a single crystal so that diffusion along grain boundaries cannot contribute. Unfortunately, the authors do not give error bars and a significant scatter in the raw data is visible. They give two diffusion coefficients, one with a very low activation energy for diffusion driven by defects created by the 100 keV ion implantation, $D = 7 \times 10^{-18} \cdot \exp\left(-\frac{0.15\text{ eV}}{kT}\right)\frac{\text{m}^2}{\text{s}}$ and a second diffusion coefficient for bulk diffusion, $D = 1.24 \times 10^{-16} \cdot \exp\left(-\frac{0.75\text{ eV}}{kT}\right)\frac{\text{m}^2}{\text{s}}$. The time constants based on these diffusion coefficients are 90 s and 8000 s, respectively. As [29] does not decide between N in the solute phase and in the nitride, these time scales were calculated assuming $\frac{c_N}{C_0} = 1$. The timescale observed in our experiments lies just between these results.

As a conclusion it can be stated that the observed N loss for heating a W_xN layer is in agreement with published diffusion coefficients. However, the published coefficients have a large scatter and do not consider the possible dependence of the diffusion coefficient on the composition, as observed for carbon diffusion in tungsten [31].

The result that diffusion only occurs above 800 K differs from the observations reported in [3], where a reduction in the nitrogen content was already observed for N implantation at 600 K. For this reason, further experiments were performed, where the sample temperature was varied during implantation. Figure 11 reveals that the N content does not only drop for an implantation above 900 K, as could be expected after the results described above. Rather, the N retention seems to decrease continuously with increasing temperature.

In detail figure 11 shows that there is almost no difference between 300 K and 800 K at low fluences. However, at 800 K the N content saturates at a much lower level than at 300 K. The implantation at 150 K seems to have a constant offset from the one at 300 K. The adsorption of N at the surface would be a possible explanation. However, the N 1*s* signal does not drop when the sample is heated to 350 K after the implantation. The implantations at 300 K and at 150 K agree within the error bars with the SDTRIM.SP simulation. In fact the SDTRIM.SP result should be compared to the 150 K measurement, since no temperature effects are considered in the BCA calculations.

From the XPS measurements it cannot be concluded whether the N content after implantation at elevated temperature is actually lower, or whether N has diffused out of the XPS range into greater depths. Therefore, the integral N content was determined with NRA. As the

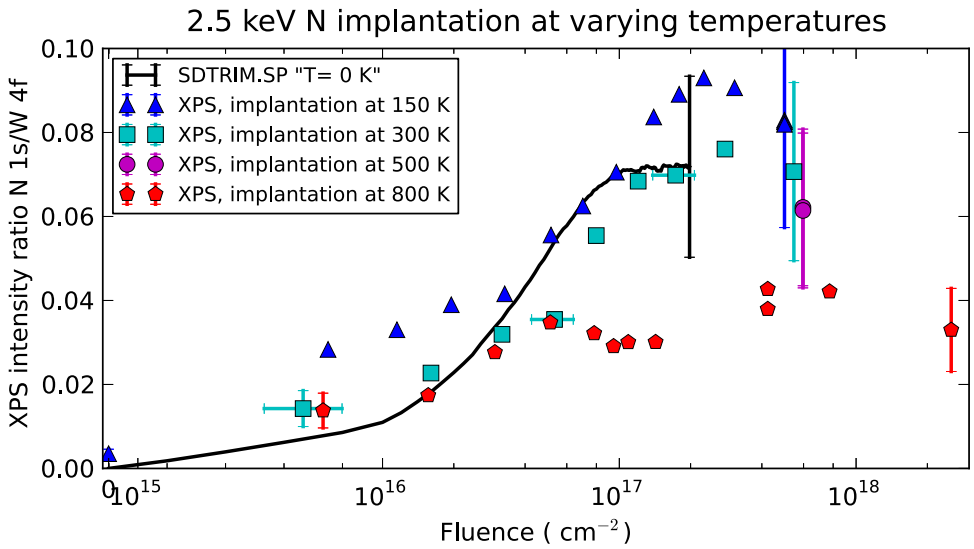

Figure 11. N 1*s*/W 4*f* intensity ratio versus fluence for different implantation temperatures.

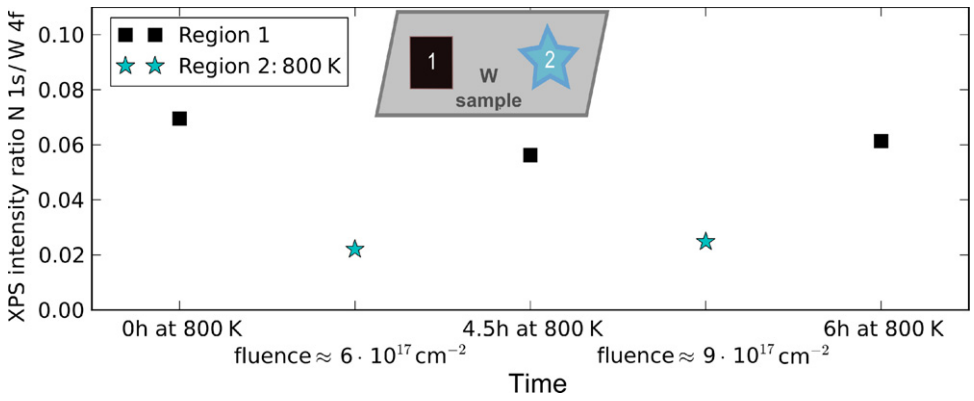

Figure 12. Subsequent implantation at ambient temperature and heating to 800 K (region 1) versus implantation into heated (region 2, 800 K) sample.

areal density decreased for the 800 K implantation to 1.5×10^{16} N cm^{-2} (from 2.3×10^{16} N cm^{-2} for ambient temperature implantation) nitrogen retention actually dropped.

To confirm the difference between (1) subsequent implantation and heating with (2) the implantation into a heated sample, a special experiment was performed: one part of a sample was implanted at ambient temperature with a N fluence of 6×10^{17} N cm^{-2}. Then the sample was heated to 800 K. XPS measurements shown in figure 12 confirm that the N signal in the corresponding region 1 (squares) did not change over several hours. Between the XPS measurements in region 1, N was implanted into another part (region 2) of the heated sample. As shown in figure 12 the N content in region 2 of the sample (stars) saturates at significantly lower N 1*s* intensities.

Due to technical limitations this measurement was performed with the non-monochromatic x-ray source. The shown intensities were derived simply with a Shirley background subtraction. Therefore these values cannot be compared quantitatively to the others given in this publication. Nevertheless, this does not affect the qualitative conclusions.

From the temperature dependence described here and in [3] it seems clear that there is a gradual reduction of the N content with increasing *implantation* temperature. There is even an indication for a continuation of this trend below ambient temperatures. Possible mechanisms causing a temperature dependent N retention from implantation are radiation enhanced diffusion [32] or a competition between diffusion and phase formation. Indications of an impact of damages created by ion bombardment on the diffusion coefficient have already been found in [29], however, for a significantly higher ion energy and for subsequent implantation and heating.

4. Simulation of D and N co-bombardment

The first wall of a nuclear fusion experiment is exposed to simultaneous bombardment of D and N with varying energies and composition. In sections 3.1 and 3.2, it was shown that the implantation of N in W and its erosion by Ar are well described by SDTRIM.SP simulations. There is only a small discrepancy between measurement and simulation for the erosion of W and W_xN layers by D. However, in the presence of heavier ions like N, the erosion is mostly dominated by the heavier ions for which the momentum transfer is much more effective. Motivated by the success of SDTRIM.SP in simulating our laboratory experiments, we simulated the N accumulation in W under D–N co-bombardment as it occurs on the first wall of a fusion experiment. The following discussion is meant to give an idea about the main results and important processes, but cannot be fully comprehensive.

The predicted fluence dependent N areal density in W is shown in figure 13. The simulations were done with varying energies of the ions and a varying beam composition. The fraction of nitrogen in the beam is shown in figure 13 by the gray numbers next to the curves. Results are given with N fractions in the beam of 100, 15 and 2% in (a), 50 and 10% in (b) and 22 and 5% in (c). The energy of the ions is indicated by the color of the line. The energy given in the legend corresponds to the energy of the deuterium ions. As N becomes multiply ionized above an electron temperature of 4 eV and the energy of impinging ions is mainly determined by the sheath acceleration, the impact energy of N was set to twice the energy of D. The maximum N concentration in the surface was set to 50% (see section 3.1). The impact angle for the presented result was, as in our experiments, 40° with respect to the surface normal.

The most notable effect of the beam composition is the required fluence to reach steady state. While it is clear that the total fluence (deuterium + nitrogen) required to reach steady state increases with decreasing N fraction in the beam, a closer look shows that also the N fluence (total fluence times N fraction) needed to reach saturation increases. This is partly due to the erosion of N by D, working against the N implantation. Finally, the increase of the N content on very long fluence scales observable for low N fractions in the beam, which in some of the simulations is still ongoing at the end of the simulated fluence interval, can be attributed to the recoil implantation of N by D. This will be discussed later in more detail. For N concentrations in the percent range and a flux of $10^{19}\,\mathrm{cm^{-2}s^{-1}}$, as is typical for the strike point region of N seeded fusion plasmas, it takes 0.1 s to 1 s until the N content saturates.

For steady state at large fluences the N content is given by the balance of N implantation and loss. The areal density in steady state varies from about $0.75 \times 10^{16}\,\mathrm{N\,cm^{-2}}$ (for low energies with pure N bombardment and high energies with low N fraction) to $1.5 \times 10^{16}\,\mathrm{N\,cm^{-2}}$ (for high energies with pure N bombardment and medium energies with

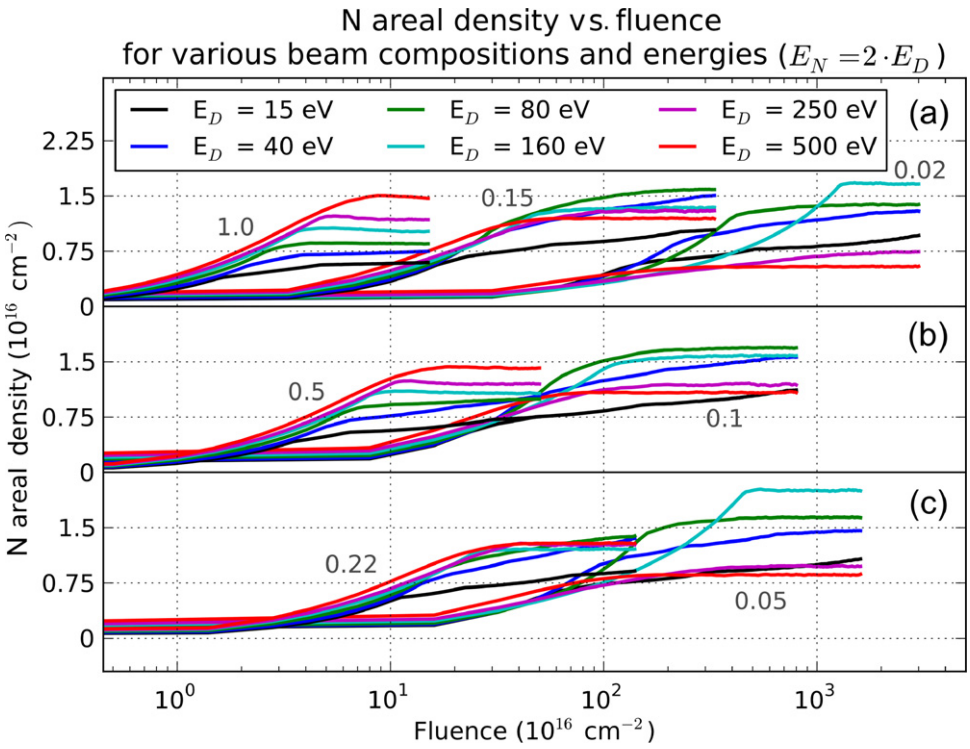

Figure 13. N areal density accumulated in a W surface versus fluence for D–N bombardment of W from SDTRIM.SP simulations. The energy of N was twice the D energy, $E_N = 2\ E_D$. The gray numbers indicate the N fraction in the beam.

low N fraction). The large N accumulation for medium energies and low N fraction in the beam is again caused by the recoil implantation of N by D, as shown in the next paragraph.

The implantation depth of N is expected to be mainly governed by the energy of the N ions. However, from a more detailed look it becomes apparent that recoil implantation of N by D significantly increases the implantation depth of N and thereby increases the N content. Figure 14 shows in both cases, D–N co-bombardment (figure 14(a)) and subsequent implantation of N and bombardment with D (figure 14(b)), a reduction of the N content directly at the surface, but also N being pushed into greater depths by D.

The dependence of the steady state N content on the beam composition is different between D energies of E_D = 500 eV and lower values. At 500 eV D energy the N content declines with increasing D fraction in the beam because the erosion by D has a larger impact than the recoil implantation. At lower energies the erosion by D becomes less effective, so for 250, 160, 80, 40 and 15 eV the N content first increases with decreasing N fraction, as more N can be recoil implanted before it becomes eroded. Around an N fraction in the beam of 10%, the N areal density reaches a maximum and then drops for even smaller fractions of N in the beam. This maximum in the N areal density for a given energy is accompanied by a change in the shape of the depth profile as can be seen in figure 15 for simulations with E_D = 160 eV. A plateau with about 15% N concentration reaching from 1 to 3 × 10^{16} cm^{-2} develops. At a depth of 5 × 10^{16} cm^{-2}, where no N is present in the pure N simulation, a peak in the N concentration with up to 50% N appears. This shape is formed by the combination of preferential erosion at the surface and recoil implantation into the depth. A peculiar feature of the simulations with

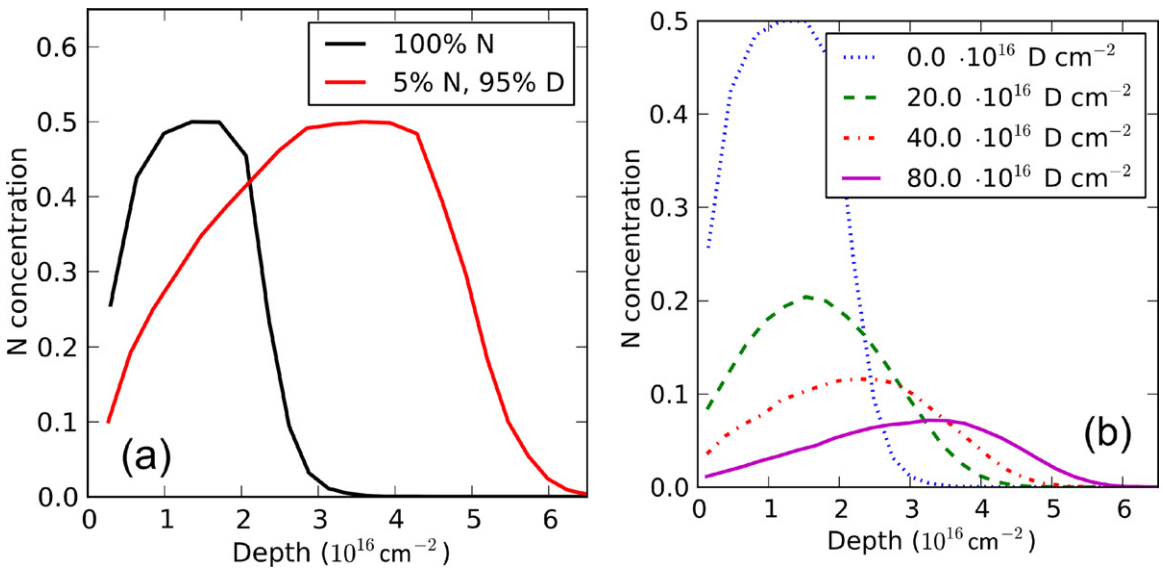

Figure 14. Calculated N depth profiles, a depth of 10^{16} cm^{-2} corresponds to about 1 nm. (a) For pure N and combined N–D bombardment at large fluence (fluence of 15×10^{16} N cm^{-2} for pure N and 1600×10^{16} N cm^{-2} for 5% N, E_D = 160 eV, E_N = 320 eV). The N concentration is limited to ⩽50%. (b) Erosion of a W_xN layer created by 320 eV N implantation followed by 160 eV D bombardment. With increasing D fluence N is eroded, but also implanted into greater depth.

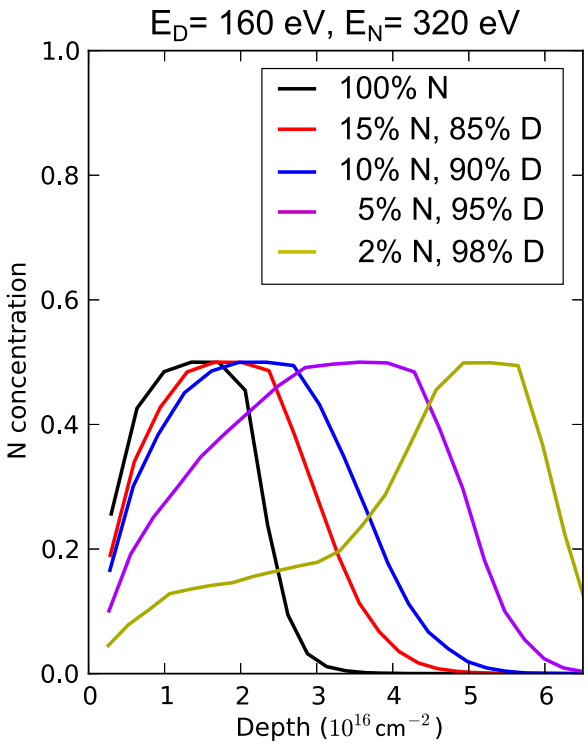

Figure 15. N depth profiles for E_D = 160 eV and E_N = 320 eV. The shape of the depth profile changes at very low N fractions in the beam. The depth profile for 5% N has the largest N areal density of all presented simulations.

160 eV D energy and low N fraction are the sharp edges in the fluence dependence. These edges are caused by the limitation of the maximum N concentration. They are especially sharp for the given parameters because this maximum concentration is reached over a large depth interval at the same time. This is in contrast to other simulations where the maximum concentration is first reached at a smaller depth interval, while recoil implantation still increases the N content in larger depth.

Due to the low momentum transfer in collisions between D and W, W is mainly sputtered by N. Even for E_D = 500 eV and an N fraction of 2% in the incident beam, more than 50% of the W erosion is due to N. No W sputtering at all takes place in the simulations with E_D = 15 eV and E_N = 30 eV. For pure N bombardment the accumulation of N reduces the W partial sputter yield by up to 30%. This shielding effect is reduced under D–N co-bombardment, as the N concentration close to the surface decreases (figure 14(a)), and totally vanishes for 2% N in the beam.

The same set of simulations as just discussed for an impact angle of 40°, was also performed with an impact angle of 60° with respect to the surface normal, as suggested in [33]. The results are not shown here but the main findings are: as could be expected from the reduced penetration depth and increased erosion associated with a larger angle, there is a reduction in the N areal densities. This reduction is rather small, about 30%, for D energies of 15, 40 and 80 eV. For the cases with 160 eV D energy and above, the N areal density is about a factor of two lower for 60° than for 40° implantation. The total W sputter yield is larger (on average by about a factor of 1.3) and the shielding effect of implanted N decreases the W erosion by less than 15%.

The simulation of simultaneous N–D bombardment already shows rather complex behavior. However, in reality the incoming particles have an energy distribution which, especially in the presence of multiple charge states, may be very broad. Furthermore, the walls are bombarded not only by deuterium and nitrogen, but also by sputtered tungsten and further impurities. Both effects may add further complexity. An open question also remains as to the mechanism for the N loss when the local N concentration exceeds 50%. The experiments showed a good agreement with SDTRIM.SP (see section 3.1) where excess N is simply removed. In the more physical picture, it is no longer thermodynamically favorable to include more N above an N concentration of 50% and the excess N diffuses towards the surface and potentially through the tungsten nitride towards the bulk. At the surface it may recombine to either N_2 or NH_3. However, the N atoms may also get bound in the unsaturated region closer to the surface (see figure 15) from where it may then be eroded by physical sputtering.

5. Summary and outlook

This work is part of a comprehensive study aiming at a better understanding of N migration and retention in the first wall of fusion experiments. We have studied the interaction of N with tungsten surfaces in well-defined laboratory experiments and computer simulations. For the comparison of our XPS measurements with simulations, a forward calculation model was developed to convert depth profiles calculated by SDTRIM.SP to XPS intensity ratios. Furthermore, the forward calculation is a valuable tool in the planning of experiments, by indicating the experimental parameters which should give the most meaningful results.

The combination of SDTRIM.SP with a forward calculation is not restricted to implantation studies but can directly be used for the simulation of sputter-depth profiles. Sputter-depth profiling is widely used for XPS measurements with a depth resolution on the

nanometer scale. However, the common, direct interpretation of the measurement is difficult and questionable due to effects like preferential sputtering and ion beam mixing. These effects are naturally included in SDTRIM.SP simulations, so that the combination of SDTRIM.SP and the forward calculation can improve the reliability of sputter-depth profile interpretation.

From a detailed analysis of W_xN XPS spectra, we determined the ratio of the actual peak intensities, which do not depend on user chosen parameters and account for the N 1*s* peak extending into the W 4*p* peak, to the intensities derived with the simple Shirley background subtraction. This allows comparison of intensities derived with the Shirley background subtraction with the forward calculations.

At low surface target temperatures the measured N accumulation agrees within the uncertainties with SDTRIM.SP simulations. For these simulations a limit of 50% was imposed on the N concentration, in agreement with the known phase of WN. Also the Ar erosion of nitride layers created by N implantation in W is in agreement with SDTRIM.SP simulations. This confirms both the N depth profile and the sputter yields calculated by SDTRIM.SP. However, the erosion of W_xN by D bombardment is by a factor of two slower than predicted by SDTRIM.SP.

Furthermore, the accumulation of N in W exhibits a complex dependency on material temperature not recovered by the SDTRIM.SP model: with increasing sample temperature, the N retention decreases steadily. In contrast, when heating an N-implanted W sample, a diffusive loss of N is only observed above 800 K. This result has not been expected and points to the occurrence of radiation enhanced diffusion. It also resolves the apparent contradiction between [3] and [7]. The slow decrease of the N inventory, especially under particle bombardment, also remedies the fear of a sudden release of large amounts of N when the WN phase may become unstable around 600 K [3].

One possible contribution to the deviation of N retention between laboratory experiments and fusion experiments [1] was identified by SDTRIM.SP simulations of D–N co-bombardment. These simulations demonstrate the importance of N recoil implantation by D. By this recoil implantation the effective penetration depth of N can be increased by more than a factor of two, thereby increasing the N retention. On the other hand a strong preferential erosion of N in the uppermost 1–3 nm is observed. For this reason the reduction of the W sputter yield due to the accumulation of N, observed for pure N bombardment [3], seems to vanish under D–N co-bombardment. The pattern of preferential erosion in the very surface of a W substrate and recoil implantation into the depth is likely not restricted to N, but may also be present for elements with even lower masses like beryllium and up to elements like iron, which is still much lighter than W.

For N concentrations in the percent range and fluxes as they are typical for the strike point region of fusion plasmas, it takes 0.1 s to 1 s until the N content in a W surface saturates.

The migration of N in fusion experiments, the consequence of wall pumping on the N flux distribution in the plasma and formation of ammonia [34] are currently studied in tokamak experiments especially at AUG and JET [35]. For these studies the retention of N in W is a key quantity. Our results from surface analysis prepared the inclusion of N in WallDYN-DIVIMP modeling [36]. WallDYN simulations finally allow a direct calculation of N migration in tokamaks and benchmarking of our results to a large number of diagnostics available in fusion devices like spectroscopic measurements, post-mortem analysis of plasma-exposed samples and residual gas analysis. Based on the results on the microscopic processes presented in this work a good agreement between WallDYN simulations and experimental measurements has been found on the scale of a fusion experiment [37].

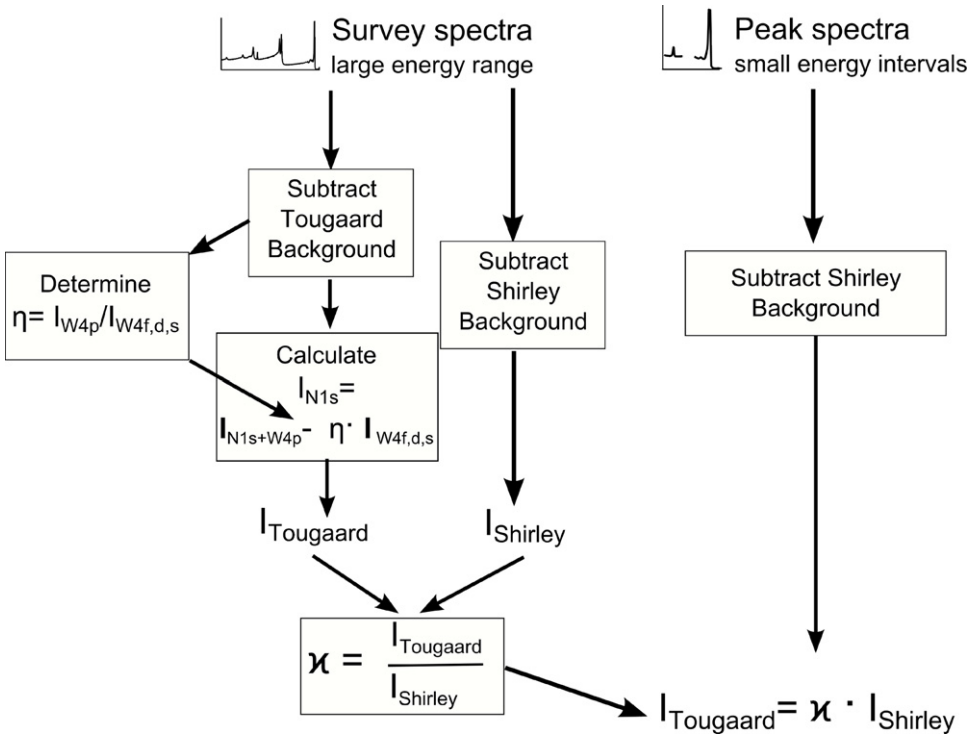

Figure 16. Sketch of the XPS evaluation.

Acknowledgments

We would like to thank colleagues from IPP for intense discussions on the interpretation of experimental results and SDTRIM.SP simulations. This project has received funding from the Euratom research and training programme 2014–2018.

Appendix A. Separation of N 1*s* and W 4*p*

The plasmon loss signal of the N 1*s* core level is superimposed by the signal of the W 4*p* core level ($4p_{1/2}$ at 490 eV and $4p_{3/2}$ at 425 eV; see figure 1(a)). However, for a consistent evaluation they have to be included in the peak intensity.

According to a forward calculation for XPS intensities, see section 2.3, the intensity ratio of the different W peaks (W 4*f*, W 4*d*, W 4*p* & W 4*s*) changes only by about one percent during N implantation. Also experimentally it was checked that the ratio of the W 4*s* intensity to the W 4*f* intensity does not change due to the N implantation. Therefore the W 4*p* intensity can be calculated from the intensity of other tungsten peaks. Then the N 1*s* intensity can be deduced by subtracting the W 4*p* intensity from the combined intensity of the N 1*s* and the W 4*p* peaks.

The ratios η of the W 4*p* intensity to the intensities of the W 4*f*, W 4*d* and W 4*s* peaks were determined from a measurement of pure tungsten. Subsequently, a set of spectra including samples that had been implanted with different energies and fluences was examined. For this set again the intensities of the W 4*f*, W 4*d* and W 4*s* peaks were determined after a Tougaard background subtraction. Furthermore, the energy interval from 388 to 525 eV was integrated, corresponding to the combined intensities of W 4*p* and N 1*s*. An estimate for the W 4*p* intensity

was calculated with the previously determined W peak intensities and η ratios W $4p$/W $4f$, W $4p$/W $4d$ and W $4p$/W $4s$. Finally, the N $1s$ intensity was obtained by subtracting the estimate for W $4p$ from the combined intensities of W $4p$ and N $1s$.

Appendix B. Estimate for solubility-controlled diffusion

In [28, 30] the expression derived for the loss of N with the solute N concentration C_0 and the diffusion coefficient D is:

$$L(t) = 2\ C_0 \sqrt{D\ t/\pi}\,. \tag{B.1}$$

From this we get an estimate for the N loss time by substituting L with the N content after implantation:

$$L \rightarrow \frac{\delta_N}{\rho_W} = \frac{\rho_N \cdot \Delta x}{\rho_W} = \frac{c_N \cdot \rho_W \cdot \Delta x}{\rho_W} = c_N \cdot \Delta x \tag{B.2}$$

where δ_N is the N areal density in the implantation zone, ρ_W the W volume density, ρ_N the N volume density, Δx the implantation zone thickness and c_N the nitrogen concentration in the implantation zone. Neglecting the factor $\frac{2}{\sqrt{\pi}}$ and solving for t gives:

$$\tau \approx \left(\frac{c_N}{C_0}\right)^2 \frac{\Delta x^2}{D}. \tag{B.3}$$

The loss time becomes longer as only the solute N contributes to the gradient driving the diffusion.

References

[1] Kallenbach A *et al* 2010 *Plasma Phys. Control. Fusion* **52** 055002
[2] Kallenbach A *et al* 2011 *J. Nucl. Mater.* **415** S19
[3] Schmid K *et al* 2010 *Nucl. Fusion* **50** 025006
[4] Dobes K, Naderer P, Lachaud N, Eisenmenger-Sittner C and Aumayr F 2011 *Phys. Scr.* **T145** 014017
[5] Soto G *et al* 2003 Tungsten nitride films grown via pulsed laser deposition studied *in situ* by electron spectroscopies *Appl. Surf. Sci.* **214** 58
[6] Jiang P-C, Lai Y-S and Chen J S 2006 Dependence of crystal structure and work function of W N x films on the nitrogen content *Appl. Phys. Lett.* **89** 122107
[7] Ogorodnikova O V *et al* 2011 *Phys. Scr.* **T145** 014034
[8] Gao L, Jacob W, Wang P, von Toussaint U and Manhard A 2014 *Phys. Scr.* **T159** 014023
[9] Lee H T, Ishida M, Ohtsuka Y and Ueda Y 2014 *Phys. Scr.* **T159** 014021
[10] Gao L 2013 private communication
[11] Shirley D A 1972 High-resolution x-ray photoemission spectrum of the valence bands of gold *Phys. Rev.* B **5** 4709
[12] Tougaard S and Sigmund P 1982 Influence of elastic and inelastic scattering on energy spectra of electrons emitted from solids *Phys. Rev.* B **25** 4452
[13] Tougaard S and Jansson C 1993 Comparison of validity and consistency of methods for quantitative XPS pak analysis *Surf. Interface Anal.* **20** 1013
[14] Tougaard S 1987 Low energy inelastic electron scattering properties of noble and transition metals *Solid State Commun.* **61** 547

[15] Behrisch R (ed) 1981 *Sputtering by Particle Bombardment I* (*Topics in Applied Physics* vol. 47) (Berlin: Springer)
[16] Möller W, Eckstein W and Biersack J P 1988 *Comput. Phys. Commun.* **51** 355
[17] Mutzke A, Schneider R, Eckstein W and Dohmen R 2011 SDTrimSP version 5.00 *IPP Report 12/08, Max-Planck-Institut für Plasmaphysik (Hrsg.)* (http://edoc.mpg.de/display.epl?mode=doc&id=552734)
[18] Dittmar T *et al* 2011 *Phys. Scr.* **T145** 014009
[19] Merzlikin S V *et al* 2008 Resolving the depth coordinate in photoelectron spectroscopy comparison of excitation energy variation vs. angular-resolved XPS for the analysis of a self-assembled monolayer model system *Surf. Sci.* **602** 755
[20] Oberkofler M and Linsmeier Ch 2010 Properties of nitrogen-implanted beryllium and its interaction with energetic deuterium *Nucl. Fusion* **50** 125001
[21] Seah M P and Gilmore I S 2001 Simplified equations for correction parameters for elastic scattering effects in AES and XPS for Q, b and attenuation lengths *Surf. Interface Anal.* **31** 835
[22] Scofield J H 1976 Hartree-slater subshell photoionization cross-sections at 1254 adn 1487 eV *J. Electron Spectrosc.* **8** 129
[23] Yeh J J and Lindau I 1985 Atomic subshel photoionization cross sections and asymmetry parameters *At. Data Nucl. Data Tables* **32** 1–155
[24] Gries W H 1996 A universal predictive equation for the inelastic mean free pathlengths of x-ray photoelectrons and auger electrons *Surf. Interface Anal.* **24** 38
[25] Seah M P, Gilmore I S and Spencer S J 2001 Quantitative XPS: I. analysis of x-ray photoelectron intensities from elemental data in a digital photoelectron database *J. Electron Spectrosc. Relat. Phenom.* **120** 93
[26] Giorginis G, Misaelides P, Crametz A and Conti M 1996 *Nucl. Instrum. Methods* B **133** 396
[27] Eckstein W, Garcia-Rosales C, Roth J and Ottenberger W 1993 Sputtering Data *IPP Report 9/82, Max-Planck-Institut für Plasmaphysik (Hrsg.)* (http://edoc.mpg.de/display.epl?mode=doc&id=394284)
[28] Keinonen J, Risnen J and Anttila A 1984 Diffusion of nitrogen in ion-implanted chromium and tungsten *Appl. Phys.* A **35** 227
[29] Bodnar O B *et al* 2006 Nitrogen diffusion parameters in ion-implanted tungsten single crystals *Phys. Solid State* **48** 10
[30] Myers S M and Langley R A 1975 Study of the diffusion of Au and Ag in Be using ion beams *J. Appl. Phys.* **46** 1034
[31] Schmid K and Roth J 2002 Concentration dependent diffusion of carbon in tungsten *J. Nucl. Mater.* **302** 96
[32] Lam N Q 1988 Ion bombardment effects on the near-surface composition during sputter profiling *Surf. Interface Anal.* **12** 65
[33] Schmid K *et al* 2010 Impact of gyro-motion and sheath acceleration on the flux distribution on rough surfaces *Nucl. Fusion* **50** 105004
[34] Neuwirth D, Rohde V and Schwarz-Selinger TASDEX Upgrade Team 2012 Formation of ammonia during nitrogen-seeded discharges at ASDEX upgrade *Plasma Phys. Control. Fusion* **54** 085008
[35] Oberkofler M *et al* 2013 First nitrogen-seeding experiments in JET with the ITER-like wall *J. Nucl. Mater.* **438** S258
[36] Schmid K, Reinelt M and Krieger K 2011 An integrated model of impurity migration and wall composition dynamics for tokamaks *J. Nucl. Mater.* **415** S284
[37] Meisl G *et al* 2014 Nitrogen retention in ASDEX upgrade *J. Nucl. Mater.* submitted